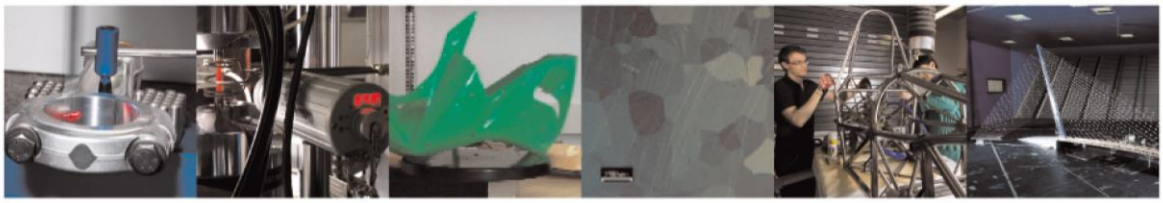

Manufacturing signature and operating conditions in a variational model for tolerance analysis of rigid assemblies

Corrado, A.; Polini, W.; Moroni, G.

This is a post-peer-review, pre-copyedit version of an article published in RESEARCH IN ENGINEERING DESIGN. The final authenticated version is available online at:
http://dx.doi.org/10.1007/s00163-017-0250-y

DIPARTIMENTO DI MECCANICA ■ POLITECNICO DI MILANO
via G. La Masa, 1 ■ 20156 Milano ■ EMAIL (PEC): pecmecc@cert.polimi.it
http://www.mecc.polimi.it
Rev. 0

Manufacturing signature and operating conditions in a variational model for tolerance analysis of rigid assemblies

Corrado A.[1], Polini W.[1] and Moroni G.[2]

[1] Università degli Studi di Cassino e del Lazio Meridionale, Dipartimento di Ingegneria Civile e Meccanica, Cassino, e-mail: polini@unicas.it

[2] Politecnico di Milano, Dipartimento di Meccanica, Milano, e-mail: giovanni.moroni@mecc.polimi.it

Abstract

The need of an univocal language for geometrical product specification considering all steps of the product life-cycle such as design, manufacturing, and inspection is inevitable. Most models for computer aided tolerancing proposed by researchers and used in industry do not fully conform with standards. Moreover, most of them make severe assumptions on observable geometric deviations and can therefore hardly handle all kinds of 3D tolerances.

These lacks inspired the idea and the development of a discrete geometry framework that is capable of considering geometric deviations of different stages of the product life cycle and is versatile regarding current and future tolerancing standards. This work uses a point cloud-based geometry representation scheme to implement the pattern left on the surfaces by a manufacturing process; then this scheme has been inserted in a variational approach for tolerance analysis. Moreover, gravity and friction among the parts to assemble have been simulated too. In this way a new Computer Aided Tolerancing (CAT) simulation tool has been developed; it approaches reality more than existing software packages do.

To verify the effectiveness of the new CAT simulation tool, it has been applied to two case studies. The obtained results have been compared with those due to a geometrical model that has been developed by simulating what happens among the parts in the actual assembly. The obtained results show how the new CAT simulation tool gives results nearer to reality than literature models do.

Keywords: tolerance analysis, manufacturing signature, friction, gravity, variational model.

1. Introduction

Even though modern manufacturing processes achieve an increasingly high accuracy, geometric deviations are observable on every manufactured part. Geometric deviations have huge influence on both the function behaviour and on the customers' quality perception of the product (Schleich et al. 2014). To control and to manage these geometric deviations along the product life-cycle, the first step is to consider during the design stage the tolerance specification, the tolerance allocation and the tolerance analysis (Armillotta and Semeraro 2011).

In the context of Computer-Aided Tolerancing (CAT), various models for the representation of dimensions and geometric tolerances and for the solution of the tolerance chains have been developed, such as vector loop (Gao et al. 1998), variational (Gupta and Turner 1993), matrix (Desrochers and Rivière 1997), Jacobian (Clemént et al. 1998), torsor (Rivest et al. 1994, Ledoux and Teissandier 2013), unified Jacobian-torsor (Desroschers et al. 2003), Polytopes (Homri et al. 2015) and the T-Map® (Davidson et al. 2002, Ameta et al. 2011). Many commercial CAT software packages support the product development in these activities for geometric product specification and tolerancing, such as 3-DCS of Dimensional Control Systems®, VisVSA of Siemens®, CETOL®, and so on (Prisco and Giorleo 2002, Shah et al. 2007). However, there is a growing interest in considering working conditions and operating windows in CAT (Anselmetti et al. 2010). These computer models for tolerance simulation and analysis make severe simplifications about observable geometric deviations, since they are reduced to rotational and translational feature defects (Polini 2012, Ameta et al. 2011). This leads to results with large ranges of uncertainty and a discrepancy between the virtual models and the observed reality (Charpentier et al. 2012). Furthermore, the tolerancing tasks in design as well as all other activities of geometric variations management should be incorporated in a complete and coherent tolerancing process (Mathieu and Ballu 2007, Dantan et al. 2003). As a response to these needs, Skin Model concept was proposed (Schleich et al. 2014, Schleich and Wartzack 2015). It is a model of the physical workpiece surface in contrast to the nominal model that is a "simple" model of the intended workpiece not taking into account inevitable geometric deviations (Schleich et al. 2014).

The research contribution of this paper is to show how to modify the variational tolerance analysis model of the literature to include the manufacturing signature and the assembly conditions, such as gravity and friction. The present paper connects a skin model scheme to a manufacturing process, in order to bring closer the CAT simulation tools to reality. The discrete geometry framework of the skin model has been represented by the pattern left on a surface by a manufacturing process. The manufacturing process leaves a pattern on the manufactured surface; this pattern is a geometrical correlation among the neighbouring points on the manufactured surface that is called signature; it has been inserted in the framework of the skin model.

To demonstrate the effectiveness of considering manufacturing signature, the variational skin model has been applied to a case study made up of three parts: a rigid box and two profiles that fit within it. The case study has been chosen simple to be solved manually, but representative since it allows to consider both dimensional and geometrical tolerances applied to the same profile. The obtained results have been compared with those due to the use of the variational model of the literature. To verify the results obtained in this way, since the experimental validation is not compatible with the 2D nature of the case study, a geometrical model has been developed. It numerically reproduces what happens in the actual assembling and it has been considered as the reference case. It adopts a point cloud-based geometry representation scheme. Finally, to validate the methodology used and applied to a simple 2D case study, a 3D case study has been considered for a further validation.

Matlab® and Minitab® software packages have been used to carry out the tolerance analysis and the statistical analysis of the obtained results respectively.

The paper is organized as follow: in Sec. 2, the modified variational model with manufacturing signature has been implemented on a 2D case study. In Sec. 3, the numerical validation is described by means of a geometrical approach with and without considering the manufacturing signature. In Sec. 4, the results are compared and discussed. Finally, in Sec. 5, a final validation of the methodology developed in previous Sections is applied on a 3D case study.

2.Variational model with manufacturing signature

The variational model proposed in (Marziale and Polini 2010, Polini 2016) has been considered and implemented in this study. The basic idea of a variational model is to represent the variability of an assembly, due to the tolerances and the assembly conditions, through a set of parameters of a mathematical model.

To create an assembly, the designer has to define the nominal shape and the dimensions of each assembly component (these information are usually contained in CAD files). Then, the designer identifies the features of each component which affect the functional requirements (functional features) and the designer assigns the dimensional and geometrical tolerances to them. Each feature has its local Datum Reference Frame (DRF), while each component and the whole assembly have their own global DRF. In nominal condition, the homogeneous transformation matrix (called TN) that allows to pass from a DRF to another is known. When real features are machined, they depart from nominal (see Figure 1). Assuming that real features maintain their nominal form (i.e. form deviations are neglected), the location of a real feature deviates from nominal, this deviation is expressed by parameters that constitute a differential homogeneous transformation matrix DT. To pass from the global DRF of the part *i* (Ri) to the local DRF of a feature *j* of part *i* (Rij), it is enough to multiply the two matrices:

$$T_{Ri \to Rij} = TN_{Ri \to Rij} \times DT_{Rij} \tag{1}$$

where $T_{Ri \to Rij}$ is the total transformation matrix to pass from the global DRF of the part *i* to the local DRF of feature *j* of part *i*; $TN_{Ri \to Rij}$ is the nominal transformation matrix to pass from the global DRF of the part *i* to the local DRF of feature *j* of part *i*; DT_{Rij} is the differential transformation matrix of the feature *j* of part *i*.

If a feature may not be directly referred to the global DRF, it is reported to it through a chain of features. To calculate the total matrix, it is enough to make the product of the single contributions as shown in Figure 2 that is valid for the case of two transformations.

Once modeled the variability of the components, they have to be assembled together. The relative location of the parts is expressed by means of parameters (that are called small kinematic adjustments) which constitute the differential homogeneous transformation matrix DA (the transformation matrix is indicated by the letter *A*=assembly to distinguish it from the matrix DT that is for the part). The total transformation to pass from the global DRF of part *i* (Ri) to the global DRF of part *l* (Rl), is simply obtained by means of the following equation (see Figure 3):

$$A_{Ri\to Rl} = AN_{Ri\to Rl} \times DA_{Ri\to Rl} = TN_{Ri\to Rij} \times DT_{Rij} \times DA_{Rij\to Rlk} \times DT^{-1}{}_{Rlk} \times TN^{-1}{}_{Rl\to Rlk} \quad (2)$$

where: $A_{Ri\to Rl}$ is the assembly matrix between part *i* and part *l*, $AN_{Ri\to Rl}$ is the assembly matrix between part *i* and part *l* in nominal condition, $DA_{Ri\to Rl}$ *is* the differential assembly matrix between part *i* and part *l*, $DA_{Rij\to Rlk}$ is the differential assembly matrix between the feature *j* of part *i* and the feature *k* of part *l*, $TN_{Ri\to Rij}$ is the nominal transformation matrix to pass from the global DRF of part *i* to the local DRF of feature *j* of part *i*, DT_{Rij} is the differential transformation matrix of feature *j* of part *i*, DT_{Rlk} is the differential transformation matrix of feature *k* of part *l*, and $TN_{Rl\to Rlk}$ is the nominal transformation matrix to pass from the global DRF of the part *l* to the local DRF of feature *k* of part *l*. The differential assembly matrix $DA_{Ri\to Rl}$ and $DA_{Rij\to Rlk}$ are hard to evaluate, since they depend by both the tolerances, that are applied to the components in contact, and the assembly conditions.

Some are the works in the literature to evaluate these differential matrices. A strategy is to model the join between the coupled parts by reconstructing the coupling sequence between the features (Li and Roy 2001). Another possibility is to impose some analytical constraints on the assembly parameters (Bernam 2005). The idea of this work is to use the manufacturing signature and the operating conditions to estimate the form parameters of the differential matrices. When all the transformation matrices are obtained, it is possible to express all the features in the same global DRF of the assembly (*R*); then the functional requirements on the assembly can be modelled. They appear as:

$$FR = f(p_1, p_2, ..., p_n) \quad (3)$$

where: *FR* is a functional requirement of the assembly, $p_1,\ldots,p_n$ are the model parameters, and *f* is the stack-up function (that is usually not linear) in the model parameters.

In order to illustrate how the manufacturing signature and the operating conditions may be inserted inside the variational model, a simple assembly composed of three parts and a synoptic scheme to highlight the procedure are shown in Figure 4 and in Figure 5 respectively. Part 1 is a hollow rectangular box. Parts 2 and 3 are two circular profiles that fit within it. A two-dimensional tolerance analysis has been carried out and the circular profiles have been considered with and without considering the manufacturing signature. The gravity and the friction have been considered during the assembly of the circular profiles with the box. The aim is the measurement of the gap *g* between the second circular profile and the top side of the box as a function of the tolerances applied to the components.

The manufacturing signature due to a turning process has been represented by means of an autoregressive (AR) moving-average (MA) model with exogenous (X) variable (ARMAX model), as proposed in (Moroni and Pacella 2008), where the manufacturing signature was mainly affected by both bi-lobe and three-lobe contours, as shown in Figure 6. This model combines a harmonic term, that stands for the systematic pattern left by the turning process on the manufactured surface, with a second-order autoregressive of the noise term, that represents the random contribution that may not be expected. Therefore, the parametric model of the identified process signature is given by:

$$Y_t = \sqrt{\frac{2}{N}} \sum_{i=2}^{3} \left[b_{2i-1} \cdot \cos\left(\frac{i \cdot t \cdot 2 \cdot \pi}{N} \right) + b_{2i} \cdot \sin\left(\frac{i \cdot t \cdot 2 \cdot \pi}{N} \right) \right] + \frac{1}{1 - a_1 B - a_2 B^2} \cdot \varepsilon_t \tag{4}$$

where $t=1,2,\ldots,N$ represent the index of data points in the sampled profile, *B* is the backshift operator, *N* is the number of equally spaced points measured on that profile. For each index *t*, Y_t represents the radial distance between the actual point and the least square substitute circle, measured at angular position $\theta_t=2\pi t/N$. Each term of the first part of Eq. (4) represents the *i*-th harmonic (*i*=2, 3), characterized by *i* undulations per revolution, by an amplitude equal to $\sqrt{2/N\left(b_{2i-1}^2 + b_{2i}^2\right)}$ and by

a phase equal to $\tan^{-1}\left(b_{2i}/b_{2i-1}\right)$. The constant term $\sqrt{2/N}$ is introduced to use normalized harmonic predictors. The parametric model in Eq.(4) is a special case of a general ARMAX model and assumes that the signature may be modelled as a weighed combination of independent predictor variables that are assumed known and constants. The parameters' vector in Eq. (4) forms a stochastic vector that has a multivariate normal distribution with the mean vector and the variance-covariance matrix, respectively, reported in Table 1. The term ε_t in Eq. (4) was modelled as Gaussian white noise with standard deviation equal to 0.374 μm.

The gap *g* has been evaluated by means of the following analytical equation, while all the details to obtain the equation are reported in Appendix:

$$g = 40 - r_1 - r_2 - d_A - d_E - \sqrt{\left(d_C + r_1 + r_2 + 40\right)^2 - \left(d_B + d_D + r_1 + r_2 - 10\right)^2} \tag{5}$$

where r_1 and r_2 are the model parameters, due to the dimensional tolerance, of the first and second circular profile respectively, d_i is the model parameters due to the form tolerance applied to the points i=A, B, C, D and E of two circular profiles in Figure 4.

This variational model has been modified to insert the manufacturing signature and the operating conditions. To do so, at first the developed approach generates two nominal circular profiles to insert into the hollow rectangular box. The circular profiles are constituted by a set of evenly distributed points, as shown in Figure 7. The amplitude of this set is equal to 7150, since this value ensures to reach a *g*-gap equal to the nominal value (1.2702 mm) when the circular profiles are considered nominal. Moreover, this value seems to be large enough to simulate the assembly without numerical simulation being too slow. To each point of the circular profile the following model has been applied:

$$\left|P_i - O\right| = R + r + d \tag{6}$$

where P_i is the generic point of the circular profile, O is the centre of the circle, R is the nominal value of the radius of the circular profile, r is the value due to the dimensional tolerance applied to the circular profiles, and d is the value due to the manufacturing signature represented by means of the

ARMAX model. The *r* parameter has a Gaussian density function with mean value equal to zero and standard deviation equal to a sixth of the dimensional tolerance range.

Once the circular profiles are generated, the first step of assembly is to insert the first circular profile into the hollow rectangular box. The developed model takes the first generated circular profile and casually rotates it. Then, it analyses the x and y coordinates of the points forming the first circular profile to identify the points of contact with the bottom and the left sides of the box (A and B in Figure 8a). Finally, the model brings the first circular profile into contact with the box in the identified points of contact.

The second step of the assembly is to insert the second circular profile into the box. The developed model takes the generated second circular profile and randomly rotates it. Then, it analyses the x and y coordinates of its points to identify the contact point with the right side of the box (D in Figure 8a). To search the contact point with the first circular profile, the model identifies the zones on the two circular profiles where the probability of contact is the highest (they are called contact zones and are shown in Figure 8a). Then, it calculates the distance between each couple of faced points that have the same x-coordinate on the two contact zones. The minimum distance (called d_{min} in Figure 8a) identifies the couple of points that are the contact points between the two circular profiles. Therefore, all the points of the second circular profile are shifted to the minimum distance along the y-axis to bring the second circular profile into contact with the first circular profile just inserted in the box, as shown in Figure 8b. The number of points equally distributed on each profile, influences the search of the contact-point between the circular profiles. In fact, larger the number of points, more accurate the searching of the contact will be between the circular profiles but, larger the number of points, longer the simulation time. However, 7150 points seem to be a good compromise.

Once assembled, the developed model evaluates the stability of the circular profiles' positions by taking into account the effect of the gravity on the circular profiles and the effect of the friction force on the contact points. If the direction of gravity force is oriented downwards (- y-axis), this analysis can be considered as a static equilibrium. The system of forces that has to be equilibrated is composed

by weight force, reaction force, and friction force applied to the points of contact among the circular profiles and the box. Therefore, to solve the balance it is necessary to translate the effect of those forces into terms of assembly specification. The general position of each circular profile is unstable if the friction force, due to the vectorial composition of the weight and the reaction forces, is close to the normal vector on the wall of the box. The angles of tilt between the reaction forces and the normal vectors are the β_i angles. If those angles' values remain smaller than the friction limit angle, the circular profile's position is stable. Otherwise, if the values of β_i become larger than the friction limit angle, the circular profile rotates until the values become smaller. From Figure 9, it is possible to see that the values of those angles and of variable g are a function of the assembly parameters α_1 and α_2 (i.e. of the random angles chosen for the rotation of the profiles to be assembled in the box) and of the values due to the dimensional and form tolerances.

Therefore, it is possible to know the stable and unstable positions of the two profiles under the action of the gravity force and the range of variability of the objective function g. To do this, the following hypotheses have been adopted to simplify the analysis:

- The friction between the parts is a static friction type. In this way, dynamic effects are ignored. Its action is expressed by means of the friction limit angle φ_{st}. Generally, this value is given by the material nature of the surfaces in contact. If the parts are made of steel which is a material typically machined by turning without considering a lubricant, the realistic values of the friction limit angle are 1.5°–2.5°.
- The inertial effects are ignored; when a position becomes unstable, the first stable position has been reached without overcoming it due to the inertial effect.
- The positioning of the second profile depends on the positioning of the first profile.

Once verified that the positions of the two circular profiles are stable, the value of the form deviation of the actual points of contact among the two circular profiles and the box have been obtained. The values of the parameters d_i of the points of contact have been substituted into Eq. (5). The value of R remains equal to 20 mm, while r is still a random variable following a Gaussian probability density

function with means equal to 0 mm and standard deviation equal to one sixth of the dimensional range. The value of the *g* gap is estimated using the Eq. (5).

Moreover, the case study has been solved also with the classical variational method of literature shown in the Eq. (5) by means of a statistical approach that considers the model parameters as statistical independent variables following Gaussian probability density functions. The value of R remains equal to 20 mm, while r_1, r_2 and d_i are random variables following a Gaussian probability density function with means equal to 0 mm and standard deviation equal to one sixth of the dimensional and form tolerance respectively, as shown in Figure 4.

3. Numerical validation

To verify the results obtained by means of the proposed model, a geometrical model has been developed for the case study. It numerically reproduces what happens in the actual assembling.

The geometrical model, which has been developed in the Matlab® environment, starts by generating two circular profiles with the manufacturing signature. Those circular profiles are randomly rotated and they are assembled into the box by means of the actual points of contact, as done in the previous paragraph. Once verified that the positions of the two circular profiles are stable, by taking into account the weight and the friction forces applied to the circular profiles, as done in the previous paragraph, the value of the *g* gap is estimated as the distance between the upper side of the box and the top side of the circular profile. An example of the profiles generated in this case is shown in Figure 9 where it is possible to see the typical form of profiles, when the manufacturing signature is applied on them, and the evaluation of the β_i angles as done in the previous paragraph.

The same geometrical approach has been applied without considering the manufacturing signature either. In this case, the approach assigns to the parameter d of Eq. (6) a Gaussian distribution with mean equal to zero and standard deviation equal to a sixth of the form tolerance (six-sigma approach). In this approach, the points of the two profiles vary independently from each other thus generating a

sudden oscillation of the profiles. An example of the circular profiles generated in this case is shown in Figure 10.

4. Results comparison and discussion

Monte Carlo simulation has been carried out by implementing 50000 runs; this value has been chosen after performing a sensitivity analysis. In particular, the sensitivity analysis has been carried out on all models by varying the number of Monte Carlo simulations and considering a scale factor F=1. The results about the standard deviations due to the sensitivity analysis are shown in Figure 11. It is evident that results are very stable if 50000 runs of Monte Carlo simulation are carried out.

Four factors F (1, 10, 50 and 100) have been used to scale the applied tolerance ranges in order to have four sets of geometrical conditions. Factor 1 involves the tolerance ranges of Figure 4, while factor 10 implies tolerance ranges ten times larger, factor 50 implies tolerance ranges fifty time larger and so on.

The normality of the obtained distributions of the gap g has been evaluated by means of Anderson-Darling test. The results are reported in Table 2 for variational models and in Table 3 for geometrical models, together with mean and standard deviation, Skewness, Kurtosis and simulation time.

The results of Table 2 and Table 3 show that increasing the tolerance ranges, when the scale factor F passes from 1 to 100, involves a decrease of the mean value and an increase of the standard deviation of the *g* gap. Even, the geometric model without manufacturing signature (model 2 in Table 3) reaches a negative mean value of the *g* gap, when F is equal to 100. This ongoing is due to the fact that when the tolerance ranges increase, the sudden oscillation of the circular profiles makes the point of contact between the circular profiles move to the peak; the next effect is the shift of the second circular profiles towards the upper side of the box up until exiting from the box. This aspect is shown in Figure 10.

The mean value of the gap *g* due to the variational model without and with manufacturing signature (models 3 and 4 in Table 2) is very near to the nominal value of 1.2702 mm for both the values of F

factor (1 and 10). The same thing happens comparing the geometrical approach with manufacturing signature (model 1 in Table 3) with the nominal value for the same values of F factor mentioned previously.

The geometrical approach without manufacturing signature (model 2) carries out a mean value of the gap that is significantly lower than the nominal value, for both the values of the F factor (1 and 10). The standard deviation of the gap *g* due to the variational model with manufacturing signature (model 4) is very near to that due to the geometrical approach with manufacturing signature (model 1) for both the values of F factor (1 and 10). It happens because the two models use the same method to find the actual points of contact among the components during the assembly, and they consider in the same way both the weight and the friction forces. Models 2 and 3 give values of the standard deviation that are significantly lower than those due to model 1:

$$\text{model 2: } \frac{\sigma_2-\sigma_1}{\sigma_1}\cdot 100=-9.6\% \ (F=1) \text{ and } -8.7\% \ (F=10) \tag{7}$$

$$\text{model 3: } \frac{\sigma_3-\sigma_1}{\sigma_1}\cdot 100=-19.2\% \ (F=1) \text{ and } -16.5\% \ (F=10) \tag{8}$$

since those models consider nominal contact points among the components during the assembly and they do not take into account the weight and the friction forces. Model 4 gives values of the standard deviation of the *g* gap that are nearest to model 1:

$$\text{model 4: } \frac{\sigma_4-\sigma_1}{\sigma_1}\cdot 100=0\% \ (F=1) \text{ and } 0.6\% \ (F=10) \tag{9}$$

These results are testified by the Levene test that has been carried out on the results (see Figure 12). The boxplots of Figure 13 show results of the measured gap *g* for all the models (model 1 is the geometrical approach with manufacturing signature, model 2 is the geometrical approach without manufacturing signature, model 3 is the variational model without manufacturing signature and model 4 is the variational model with manufacturing signature) and for the two scale factors. The same figure reports the nominal value of the gap *g* (equal to 1.2702 mm), the boxplots of the gap *g* as a result of the Monte Carlo simulations and the tolerance range due to the worst case approach (classical

approach in tolerance analysis). All the four models give a distribution of the gap *g* completely contained inside the worst-case tolerance range.

Models 1, 2 and 4 have comparable simulation times that are 600 times higher than the time required for simulation 3. In particular, the model 3 appears a good choice in terms of simulation time, if it is possible to neglect a decrease of about 19% in the estimation of gap *g*. It is evident that model 4 is the nearest to reference model 1.

5. Final validation on a 3D case study

To validate the used methodology a further 3D case study has been considered. The considered 3D case study is constituted by three components: a hollow box and two spheres, as shown in Figure 14. The aim is the measurement of the gap *g* between the upper sphere and the top side of the box as a function of the tolerances applied to each component. The manufacturing signature on each sphere has been represented by means of a Simultaneous Autoregressive Model of first order SAR(1). Traditional time series models, as the ARMAX model adopted in the 2D case, can represent correlation only along a single direction. The SAR(1) model instead can consider the spatial structure of the lattice defined by the triangulation of the points on the surface of the sphere at their nominal coordinates to generate a spatially correlated set of deviations from perfect sphericity.

In a SAR(1) model the deviations from perfect sphericity are simulated by means of the following equation:

$$d = \left(I - G\right)^{-1} \varepsilon \tag{10}$$

where I is the identity matrix, G is a weight matrix and $\varepsilon \sim N(0,\sigma^2 I)$ is a white noise with σ is equal to 0.0024 mm. In particular, $G = \rho W$, where ρ is a correlation coefficient. Higher values of ρ denote a higher degree of spatial correlation among nearby points. Its value is 0.9. W is a neighbourhood matrix defined based on the triangulation of the points on the surface of the sphere. In particular,

$$W_{ij} = \frac{\frac{I_{ij}}{d_{ij}}}{\Sigma_k \frac{I_{kj}}{d_{kj}}} \tag{11}$$

in which d_{ij} is the Cartesian distance between the P_i and the P_j points of the sphere, and I_{ij} is an indicator variable, which denotes whether points i and j are neighbours, that is

$$I_{ij} = \begin{cases} 1, \text{ if point i and j belong to a same triangle} \\ 0, \text{ otherwise} \end{cases} \tag{12}$$

The gap g has been evaluated by means of the following analytical equation:

$$\begin{aligned} g = 1.2702 - \big[& d_A + r_1 + \left(3200 + 60d_B + 40d_c - 40d_E + 60d_F + 100r_1 - 40d_B + \right. \\ & -40d_C + 80d_{D1} + 80d_{D2} + 100r_2 + 2d_{D1}d_{D2} - 2d_B r_1 - 2d_C r_1 + 2d_{D1}r_1 + 2d_{D2}r_1 + \\ & +2d_{D1}r_2 + 2d_{D2}r_2 + 40\left(d_c + r_1\right) - 40\left(-d_B - r_1\right) + 2r_1 r_2 - d_B\left(-2d_B - 2r_1\right) + \\ & +d_C\left(2d_c + 2r_1\right) + r_1\left(2d_c + 2r_1\right) - r_1\left(-2d_B - 2r_1\right) - d_B^2 - d_C^2 + d_{D1}^2 + d_{D2}^2 - r_1^2 + \\ & \left. +r_2^2 - \left(d_c + r_1\right)^2 - \left(+d_B + r_1\right)^2 - 1700\right)^{0.5} - 58.73\big] - 20 - r_2 - d_G \end{aligned} \tag{13}$$

where r_1 and r_2 are the model parameters, due to the dimensional tolerance, of the first and second sphere respectively, d_i is the model parameters due to the form tolerance applied to the points i=A, B, C, D, E, F and G of two spheres in Figure 14. The Eq. (13) was obtained with the same approach reported in Appendix and used on the 2D case study but considering the third dimension in the equations of features and constraints.

This variational model has been modified to insert the manufacturing signature. To do so, at first the developed approach starts by generating spheres. Each sphere has been simulated by a set of evenly distributed points. The amplitude of this set is equal to 235822. To each point of the sphere it has been applied the model of Eq. (6). Also in this case, P_i and O are the generic point and the centre of the sphere, R is the nominal value of the radius of the sphere, r is the value due to the dimensional tolerance applied to the sphere, and d is the value due to the manufacturing signature represented by means of the SAR(1) model. The r parameter has a Gaussian density function with mean value equal to zero and standard deviation equal to a sixth of the dimensional tolerance range.

Once the spheres are generated, these spheres are randomly rotated around the X_i, Y_i and Z_i axes of a reference system that is placed in the centre of gravity of each sphere that has been calculated by the arithmetic mean of all the points' coordinates. Then, an absolute X-Y-Z reference system is placed at the intersection among the left, the back and the bottom sides of the box, as shown in Figure 14. The coordinates of the points constituting the first sphere are analyzed then the first sphere is brought into contact with the bottom, the left and the back sides of the box (A, B, C in Figure 14).

Therefore, the coordinates of the points constituting the second sphere are analyzed to identify the points of contact with the sides of the box, for example with the right and the back sides of the box (F and E in Figure 14). To identify the point of contact with the first sphere, the zones on the spheres, where the probability of contact is the highest, are defined. They are a surrounding of the nominal point of contact. Then, the couples of faced points have been identified, as those points having the same x and z coordinates on the two contact zones. The minimum distance between each couple of faced points (called d_{min} in Figure 15a) defines the couple of points that are the points of contact between the two spheres. All the points of the second sphere are shifted by the minimum distance along Y-axis to bring the second sphere into contact with the first sphere just inserted in the box, as shown in Figure 15b. Once assembled, it is evaluated if the general position of each sphere is stable. The condition of balance among the forces is expressed by requiring that they pass through the same point. Therefore, considering the weight force applied in the centre of gravity of the clouds (G_1 and G_2 in Figure 15b), the reactions are applied to the points of contact and they are directed toward the centre of gravity of the sphere. The angles among these reactions and the normal vectors to the surfaces are $\beta_1, \beta_2, \beta_3, \beta_4, \beta_5, \beta_6$, as shown in Figure 15b. These six angles should have a value smaller than the static friction limit angle in order to have a stable position of the sphere as explained in Sec. 2. Once verified that the positions of the two spheres are stable, the coordinates of the contact points are transformed into coordinates associated to the DRF of each sphere. Then, they are used to enter inside the array of the generated point-cloud to read the corresponding form deviations. The values of the model parameter of the points of contact have been substituted into Eq. (13). Finally, the value

of the gap *g* is estimated as the distance between the upper side of the box and the top side G of the second sphere.

The 3D case study has been solved also with the classical variational method of literature shown in the Eq. (13) by means of a statistical approach that considers the model parameters as statistical independent variables following Gaussian probability density functions. The values r_1, r_2 and d_i are random variables following a Gaussian probability density function with means equal to 0 mm and standard deviation equal to one sixth of the dimensional and form tolerance respectively, as shown in Figure 14.

Also in this case, a geometrical model has been developed for the 3D case study. The geometrical model starts by generating two spheres with the manufacturing signature. Those spheres are randomly rotated and they are assembled into the box by means of the actual points of contact. Once verified that the positions of the two spheres are stable, by taking into account the weight and the friction forces applied to the circular profiles, the value of the *g* gap is estimated as the distance between the upper side of the box and the top side of the sphere.

Monte Carlo simulation has been carried out by implementing 10000 runs and considering only a scale factor F=1. The results are reported in Table 5 together with mean, standard deviation, Skewness, Kurtosis and simulation time.

All the three models give a distribution of the gap *g* completely contained inside the worst case tolerance range (1.2702±0.0997). The normality of the obtained distributions of the gap *g* has been evaluated by means of Anderson-Darling test. The variational model with manufacturing signature is very near to the geometrical model in terms of both mean value and standard deviation. The variational model overestimates slightly the mean value of the gap *g*, even if it is negligible. It underestimates the standard deviation of about 13% because the variaional model does not take into account the correlation among the points of the spheres.

The geometrical model and the variational model with manufacturing signature have comparable simulation times (108000 s) that are significantly higher than the time required for simulation the

variational model (few seconds). Therefore, this last one appears a good choice in terms of simulation time, if it is possible to neglect a decrease of about 13% in the estimation of gap *g*.

6. Conclusions

The first effort of this work was to integrate the manufacturing signature in a model of the literature for tolerance analysis: the variational one, in order to bring closer a CAT simulation tool to reality. The second effort was to develop a geometrical model to simulate the assembly of parts with geometrical deviations that are correlated according to the manufacturing process signature, in such a way to satisfy the Geometric Dimensioning and Tolerancing (GD&T) standards, and in presence of the agents operating during the assembly, such as friction and gravity.

On the 2D case study, the results show that the variational model with the manufacturing signature and the operating conditions allows to better reproduce the actual assembling of machined circular profiles in presence of weight and friction forces. In fact, the mean value and the standard deviation of this model are statistically equal to those of the geometrical approach that considers the manufacturing signature and the operating conditions. The variational model of literature without the manufacturing signature underestimates the tolerance range of the gap g by about 19%, even if its simulation time is only 19 s. The geometrical approach without manufacturing signature does not reproduce what happens in reality; it is due to the rapid variation of the discretized profiles, due to the considered Gaussian distributions of the dimensional and geometrical deviations. The variational model has a general structure that may be easily applicable to any kind of assemblies by requiring a short computational time, at the same time guaranteeing a good agreement with the reference geometrical model. The geometrical model, that has been built to validate the variation model with and without manufacturing signature and operative conditions, requires a consistent modelling effort and cannot be easily implement in CAT software.

Same conclusions have been obtained on the 3D case study as a further validation of the methodology used.

This work represents a first step towards the integration of design and manufacturing, since it tries to integrate in a design tool, such as the tolerance analysis, a typically manufacturing signature, an innate property of every manufacturing process that characterizes the correlation among the points of the same profile. The manufacturing signature and the operating conditions may influence the tolerance range of the functional requirement drastically also in simple case studies as those used in this work. The drawback of all the models that involves the manufacturing signature and the operating conditions is the simulation times, which may be overcome by parallel computing techniques, which are currently object of further study.

Appendix

The linear features of the box have been called L_1, L_2, L_3, and L_4, while C_1 and C_2 are the two circular profiles. The DRFs (Datum Reference Frame) assigned to the features of the parts and to the whole assembly are shown in Figure 16. The assembly DRF is the global DRF of the box. It is possible to evaluate the nominal transformations matrices that allow passing among the different DRFs and, giving the model parameters, evaluating the differential transformation matrices to pass from the nominal local DRF to the local real DRF. In a previous work, all differential transformation matrices were presented in detail (Polini and Moroni 2015). Consequently, it is possible to evaluate the equations of the features in the DRF of the part. The equations of the features are:

$$L_1: -r_{z1}X + Y + \left(25r_{z1} - t_{y1}\right) = 0 \tag{A1}$$

$$L_2: -X - r_{z2}Y + \left(50 - t_{y2} + 40r_{z2}\right) = 0 \tag{A2}$$

$$L_3: r_{z3}X - Y + \left(80 - t_{y3} - 25r_{z3}\right) = 0 \tag{A3}$$

$$L_4: X + r_{z4}Y - \left(40r_{z4} + t_{y4}\right) = 0 \tag{A4}$$

$$C_1: \left(X - \Delta X_{12} - O_{12X}\right)^2 + \left(Y - \Delta Y_{12} - O_{12Y}\right)^2 = \left(R_1 + r_1 + d_1\right)^2 \tag{A5}$$

$$C_2: \left(X - \Delta X_{13} - O_{13X}\right)^2 + \left(Y - \Delta Y_{13} - O_{13Y}\right)^2 = \left(R_2 + r_2 + d_2\right)^2 \tag{A6}$$

where r_{zi} and t_{yi} are the rotation and the translation parameters of the generic side L_i of the box measured in theirs DRF respectively, R_1 and R_2 are the nominal values of the circular profiles' radius. The model parameters, due to the dimensional tolerance, of the first and second circular profile are r_1 and r_2 respectively, d_1 and d_2 are the model parameters due to the form tolerance applied to the points A, B, C, D and E of two circular profile. (O_{12X}, O_{12Y}) and (O_{13X}, O_{13Y}) are the centres nominal coordinates of two circular profiles. ΔX_{12} and ΔY_{12} are the assembly parameters of the first profile on the rectangular box, ΔX_{13} and ΔY_{13} are the assembly parameters of the second profile on the previous parts.

The assembly issue is solved by applying the assembly conditions to the obtained expressions of all the features in the global DFR. The functional requirement is evaluated between the feature L_3 of the box and the feature C_2 of profile 2, as shown in Figure 4. Profile 1 is assembled to the box by means of two constraints of the cylinder slider type: the first between the feature C_1 and the feature L_1, and the second between the feature C_1 and the feature L_4. For this type of constraint, the related mathematical expression is (Polini and Moroni 2015):

$$n_x t_x + n_y t_y + c_x n_x + c_y n_y + c - (d + r) = 0 \tag{A7}$$

Therefore, the two equations of constraint are:

$$\mathrm{C_1\text{-}L_1}: -r_{z1}\left(\Delta X_{12} + 20\right) + \left(\Delta Y_{12} + 20\right) + \left(25 r_{z1} - t_{y1} - 20 - r_1 - d_1\right) = 0 \tag{A8}$$

$$\mathrm{C_1\text{-}L_4}: \left(\Delta X_{12} + 20\right) + r_{z4}\left(\Delta Y_{12} + 20\right) - \left(40 r_{z4} + t_{y4} + 20 + r_1 + d_1\right) = 0 \tag{A9}$$

By solving system of Eqs (A8)-(A9), it results:

$$\Delta X_{12} = \left[t_{y4} + r_1 + d_B + r_{z4}\left(40 + 5 r_{z1} - t_{y1} - r_1 - d_A\right)\right] / \left(1 + r_{z1} r_{z4}\right) \tag{A10}$$

$$\Delta Y_{12} = r_{z1}\Delta X_{12} - 5 r_{z1} + t_{y1} + r_1 + d_A \tag{A11}$$

which are the solutions of the assembly problem between profile 1 and the box.

The profile 2 is assembled on the subassembly box-profile 1 by means of a constraint of cylinder slider type between the feature C_2 and the feature L_2 and by means of a constraint of cylinder-cylinder type between the features C_2 and C_1. For this last constraint, the assembly equation is:

$$t_x^2 + t_y^2 + 2\left(c_{2x} - c_{1x}\right)t_x + 2\left(c_{2y} - c_{1y}\right)t_y + \left(c_{2x} - c_{1x}\right)^2 + \left(c_{2y} - c_{1y}\right)^2 - \left(r_1 + r_2 + d_1 + d_2\right)^2 = 0 \tag{A12}$$

Therefore, the two equations of constraint are:

$$\text{C}_2\text{-L}_2\text{:} -\left(\Delta X_{13} + 30\right) - r_{z2}\left(\Delta Y_{13} + 58.73\right) + \left(50 - t_{y2} + 40r_{z2} - 20 - r_2 - d_2\right) = 0 \tag{A13}$$

$$\text{C}_1\text{-C}_2\text{:} \left(\Delta X_{13} - \Delta X_{12} + 10\right)^2 + \left(\Delta Y_{13} - \Delta Y_{12} + 38.73\right)^2 - \left(40 + r_1 + d_1 + r_2 + d_2\right) = 0 \tag{A14}$$

By solving system of Eqs (A13)-(A14), it results:

$$\Delta X_{13} = -r_{z2}\Delta Y_{13} - a \tag{A15}$$

$$\Delta Y_{13} = b + \sqrt{\left(b^2 - c\right)} \tag{A16}$$

where a, b, and c are:

$$a = 18.73r_{z2} + t_{y2} + r_2 + d_D \tag{A17}$$

$$b = \left[r_{z2}\left(10 - a - \Delta X_{12}\right) - 38.73 + \Delta Y_{12}\right] / \left(1 + {r_{z2}}^2\right) \tag{A18}$$

$$c = \left[\left(10 - a - \Delta X_{12}\right)^2 + \left(38.73 - \Delta Y_{12}\right)^2 - \left(40 + r_1 + r_2 + d_C\right)^2\right] / \left(1 + {r_{z2}}^2\right) \tag{A19}$$

That is the solution of the assembly problem between profile 2 and the subassembly box-profile 1. Now, by evaluating the smallest oriented distance between a profile with centre (c_x, c_y) and radius r, and a line of equation $n_x x + n_y y + c = 0$, it is possible to evaluate the functional requirement g:

$$\text{distance} = n_x c_x + n_y c_y + c - r_2 - d_2 \tag{A20}$$

$$g = 1.2702 + r_{z3}\Delta X_{13} - \Delta Y_{13} + 5r_{z3} - t_{y3} - r_2 - d_E \tag{A21}$$

The parameters r_{zi} and t_{yi} of the sides of the box are equal to zero, since the box has been considered nominal. Therefore the Eq. (A21) becomes:

$$g = 40 - r_1 - r_2 - d_A - d_E - \sqrt{\left(d_C + r_1 + r_2 + 40\right)^2 - \left(d_B + d_D + r_1 + r_2 - 10\right)^2} \tag{A22}$$

Acknowledgments

This research received no specific grant from any funding agency.

References

Ameta G, Serge S, Giordano M (2011) Comparison of spatial math models for tolerance analysis: tolerance-maps, deviation domain, and TTRS. J. Comput Inf Sci Eng 11(2).

Anselmetti B, Chavanne R, Yang J-X, Anwer N (2010) Quick GPS: a new cat system for single-part tolerancing. Comput Aided Des 42(9):768-780.

Armillotta A, Semeraro Q (2011) Geometric tolerances-impact on product design, quality inspection and statistical process monitoring. In: Colosimo BM, Senin N (eds) Geometric tolerance specification, Springer, pp. 3-38.

Berman YO (2005) Shape and Position Uncertainty in Mechanical Assembly Ph. Thesis, The Hebrew University, Jerusalem, Israel.

Charpentier F, Ballu A, Pailhes J (2012) A scientific point of view of a simple industrial tolerancing process. In: Proceedings of the 12th CIRP Conference on computer aided tolerancing, 2012.

Clément A, Riviére A, Serré P, Valade C (1998) The TTRSs: 13 Constraints for Dimensioning and Tolerancing, In: ElMaraghy HA (ed) Geometric Design Tolerancing: Theories, Standards and Applications, Chapman and Hall, London, pp. 123–131.

Dantan J-K, Anwer N, Mathieu L (2003) Integrated tolerancing process for conceptual design. CIRP Ann Manuf Technology 52(1):135-138.

Davidson JK, Mujezinovic A, Shah JJ (2002) A New Mathematical Model for Geometric Tolerances as Applied to Round Faces. ASME J Mech Des 124:609–622.

Desrochers A, Rivière A (1997) A matrix approach to the representation of tolerance zones and clearances. Int J Adv Manuf Technol 13: 630-636.

Desrochers A, Ghie W, Laperrière L (2003) Application of a unified Jacobian-Torsor model for tolerance analysis. ASME J Comput Inf Sci Eng 3: 1-13.

Gao J, Chase KW, Magleby SP (1998) General 3-D tolerance analysis of mechanical assemblies with small kinematic adjustments. IIE Trans 30:367–77.

Ghie W (2010) Tolerance Analysis Using Jacobian-Torsor Model: Statistical and Deterministic Applications. Modeling Simulation and Optimization - Tolerance and Optimal Control, Shkelzen Cakaj (Ed.), InTech.

Gupta S, Turner JU (1993) Variational solid modelling for tolerance analysis. IEEE Comput Graph Applicat 13:64-74.

Homri L, Teissandier D, Ballu A (2015) Tolerance analysis by polytopes: Taking into account degrees of freedom with cap half-spaces. Comput Aided Des 62:112-130.

Ledoux Y, Teissandier D (2013) Tolerance analysis of a product coupling geometric and architectural specifications in a probabilistic approach. Res Eng Design 24:297-311.

Li B, Roy U (2001) Relative positioning of Toleranced Polyhedral Parts in an Assembly. IIE Trans 33:323-336.

Marziale M, Polini W (2010) A new model based on variational solid modelling. In: Proceedings of the ASME 2010, 10th Biennial Conference on Engineering Systems, Instanbul, Turkey, July 12-14.

Mathieu L, Ballu A (2007) A model for a coherent and complete tolerancing process. In: Davidson JK (ed) Models for computer aided tolerancing in design and manufacturing, Netherlands, Springer, 35-44.

Moroni G, Pacella M (2008) An Approach Based on Process Signature Modeling for Roundness Evaluation of Manufactured Items. ASME J Comput Inf Sci Eng 8:021003.

Polini W (2012) Taxonomy of models for tolerance analysis in assembling. Int J Prod Res 50(7):2014-2029.

Polini W, Moroni G (2015) Manufacturing signature for tolerance analysis. J Comput Inf Sci Eng 15(6): 5 pages.

Polini W (2016) More geometric tolerances on the same surface for a variational model. Int J Eng Tech. 8(1):526-535.

Prisco U, Giorleo G (2002) Overview of Current CAT Systems. Integr Comput Aid Eng 9(4):373-397.

Rivest L, Fortini C, Morel C (1994) Tolerancing a Solid Model With a Kinematic Formulation. Comput-Aided Design 26:465–476.

Schleich B, Anwer N, Mathieu L, Wartzack S (2014) Skin Model Shapes: a new paradigm shift for geometric variations modelling in mechanical engineering. Computer Aided Design 50:1-15.

Schleich B, Wartzack S (2015) Evaluation of geometric tolerances and generation of variational part representatives for tolerance analysis. Int J Adv Manuf Technol 79(5-8):959-983.

Shah J J, Ameta G, Shen Z and Davidson J (2007) Navigating the Tolerance Analysis Maze. Comput Aided Des & Appl 4 (5):705-718.

Figure captions

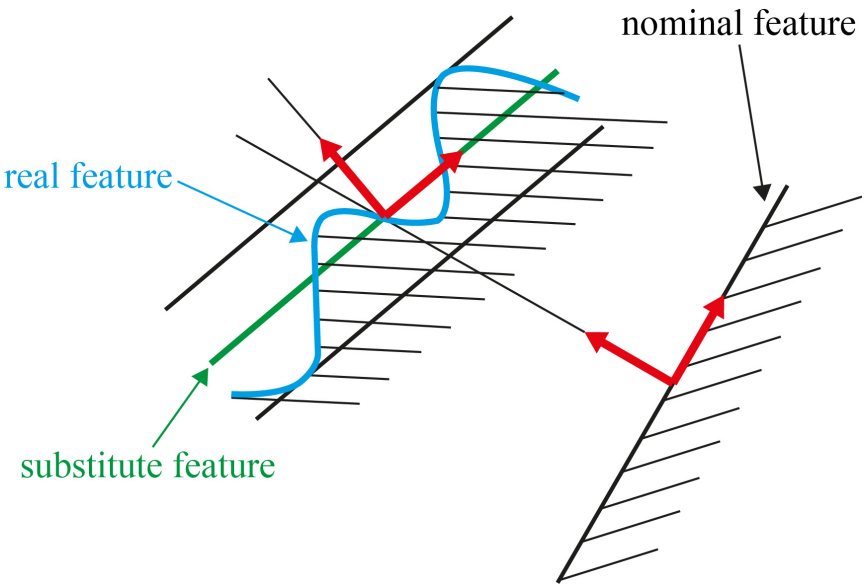

Figure 1. Nominal, real and substitute features.

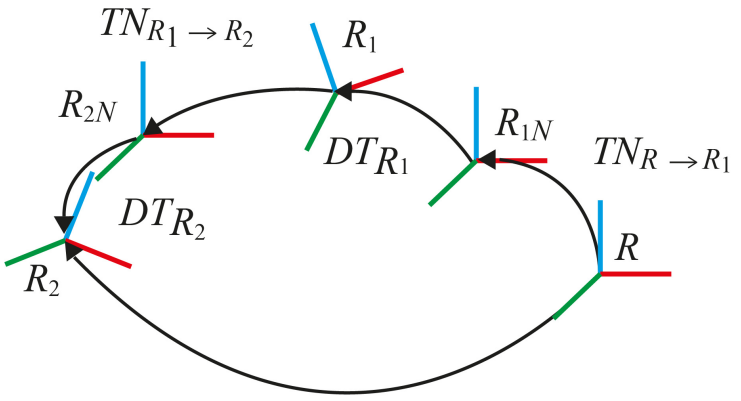

$$T_{R \rightarrow R2} = TN_{R \rightarrow R1} \cdot DT_{R1} \cdot TN_{R1 \rightarrow R2} \cdot DT_{R2}$$

Figure 2. Model of a stack-up function in a part.

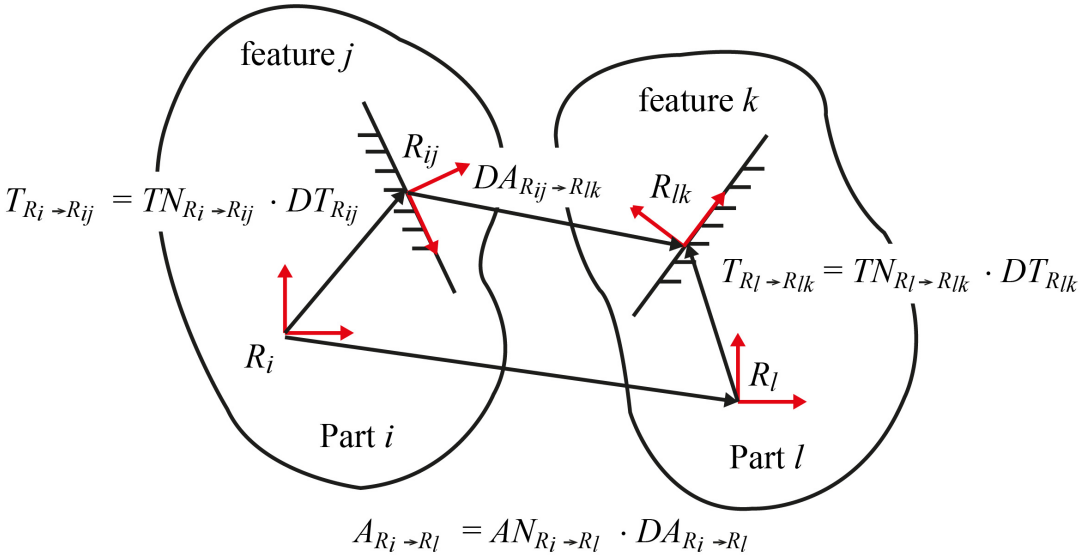

Figure 3. Model of a stack-up function between two parts.

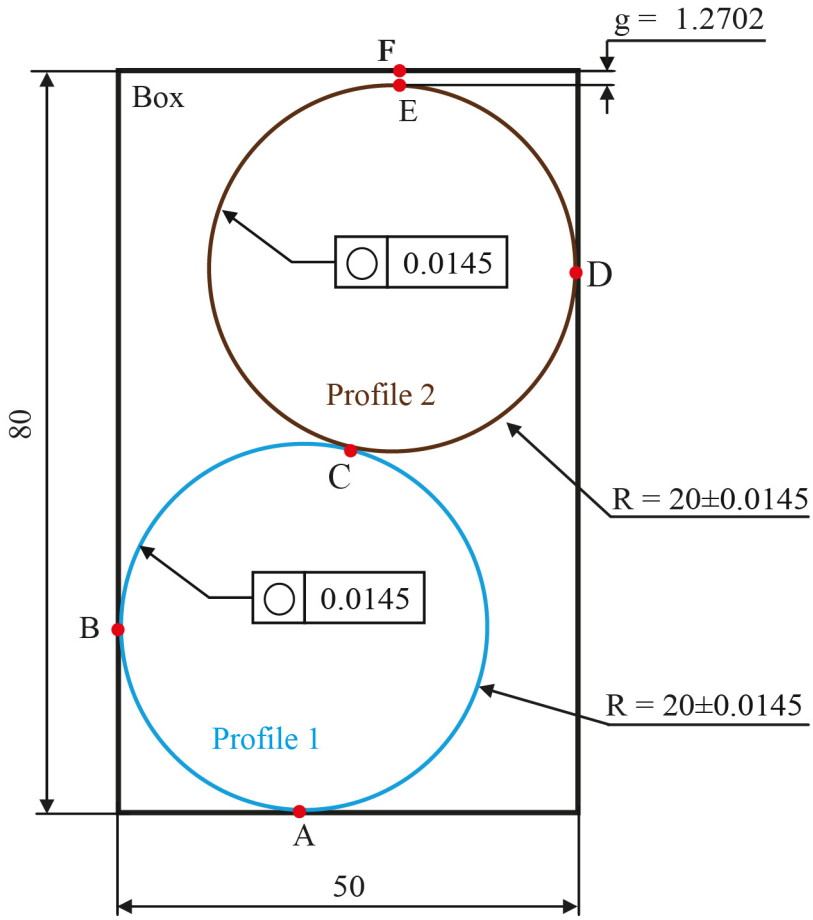

Figure 4. Case study (all dimensions and tolerances are in mm).

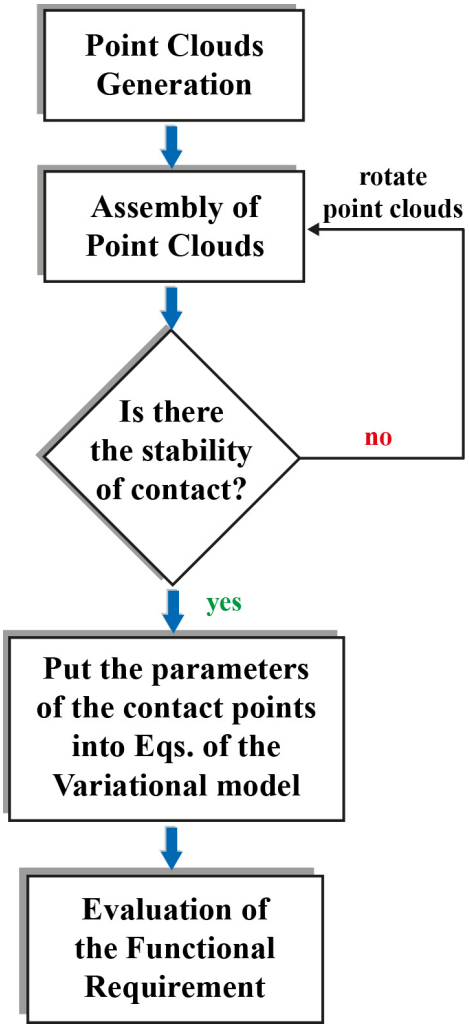

Figure 5. Scheme of the new point cloud variational model with operating conditions.

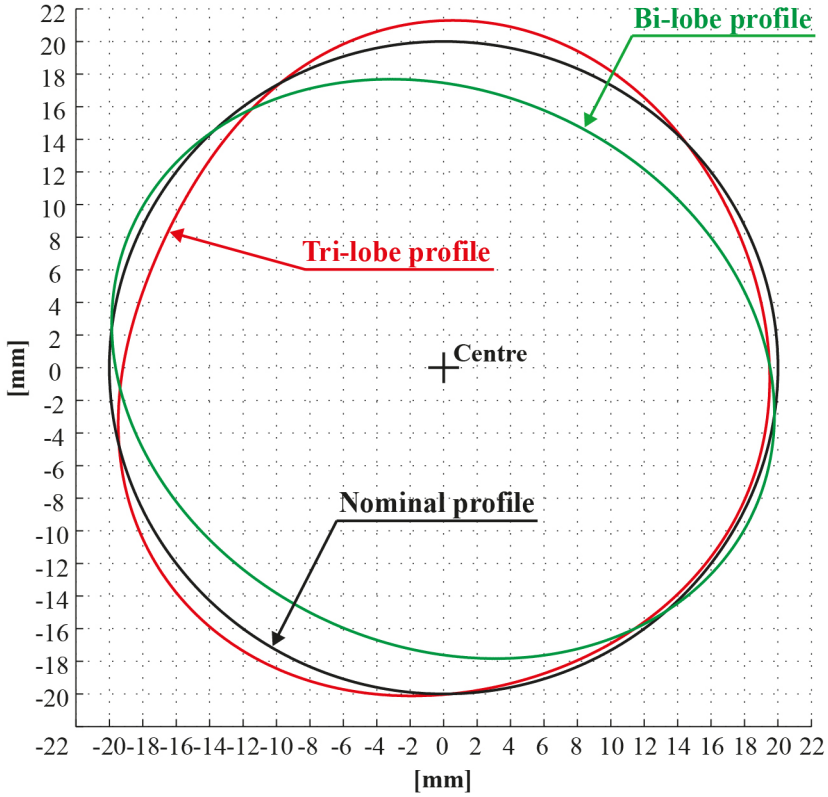

Figure 6. Comparison between a nominal circular profile and bi-lobe and tri-lobe profiles.

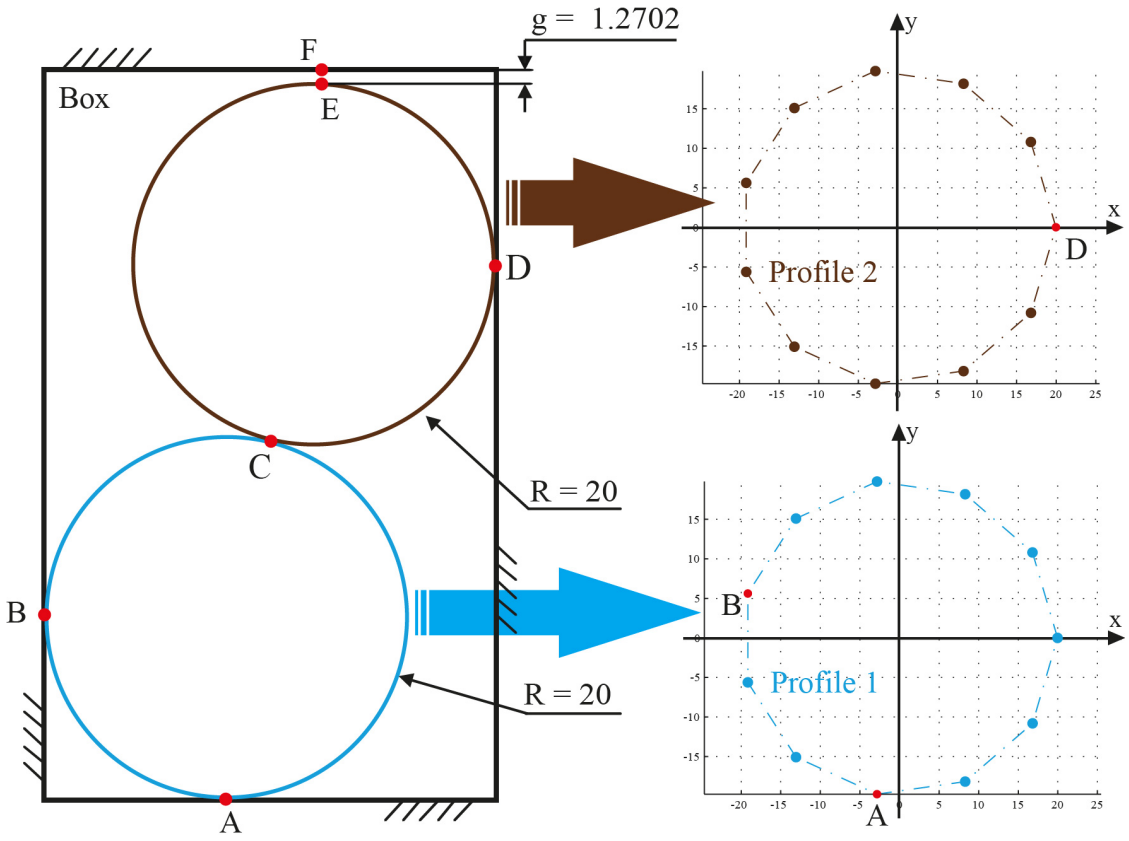

Figure 7. Discretization of the two circular profiles.

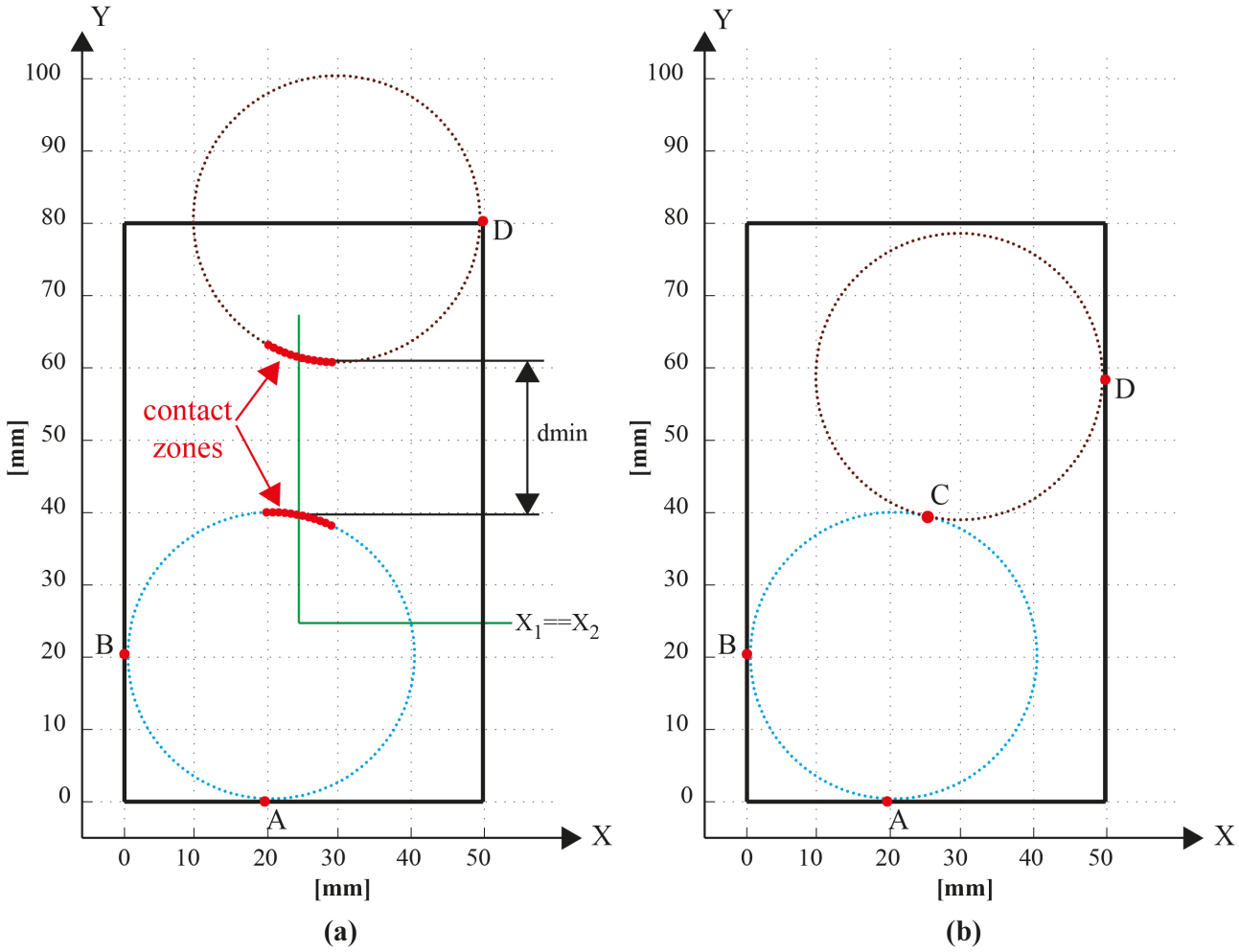

Figure 8. Approach to bring the two circular profiles into contact: a) contact zone and minimum distance between two circular profiles; b) contact in C point.

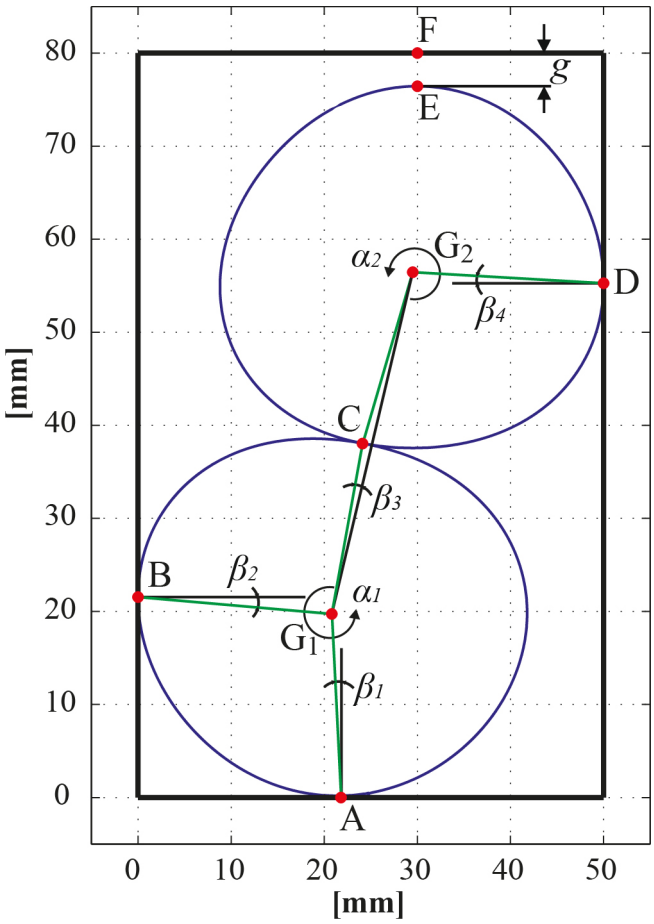

Figure 9. Tilt angles of the two circular profiles.

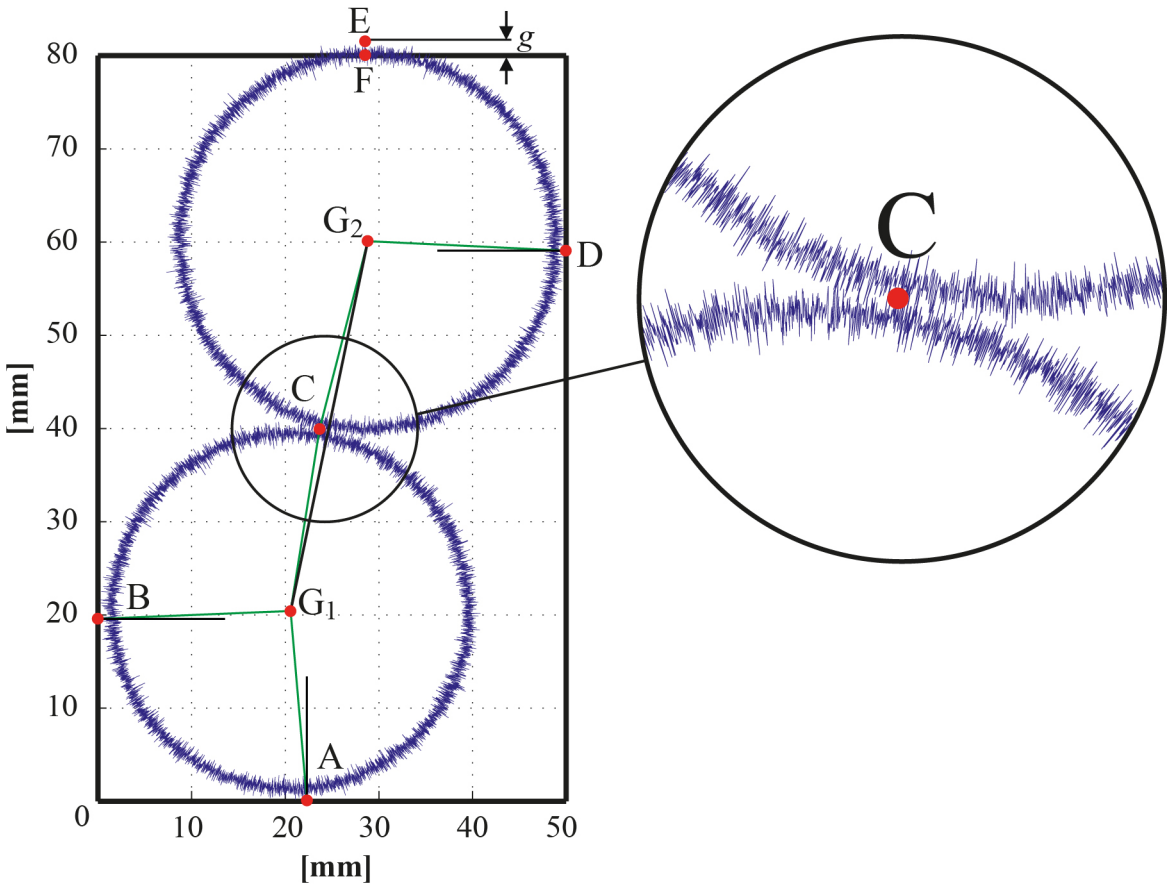

Figure 10. Example of circular profiles without manufacturing signature (amplified 100 times).

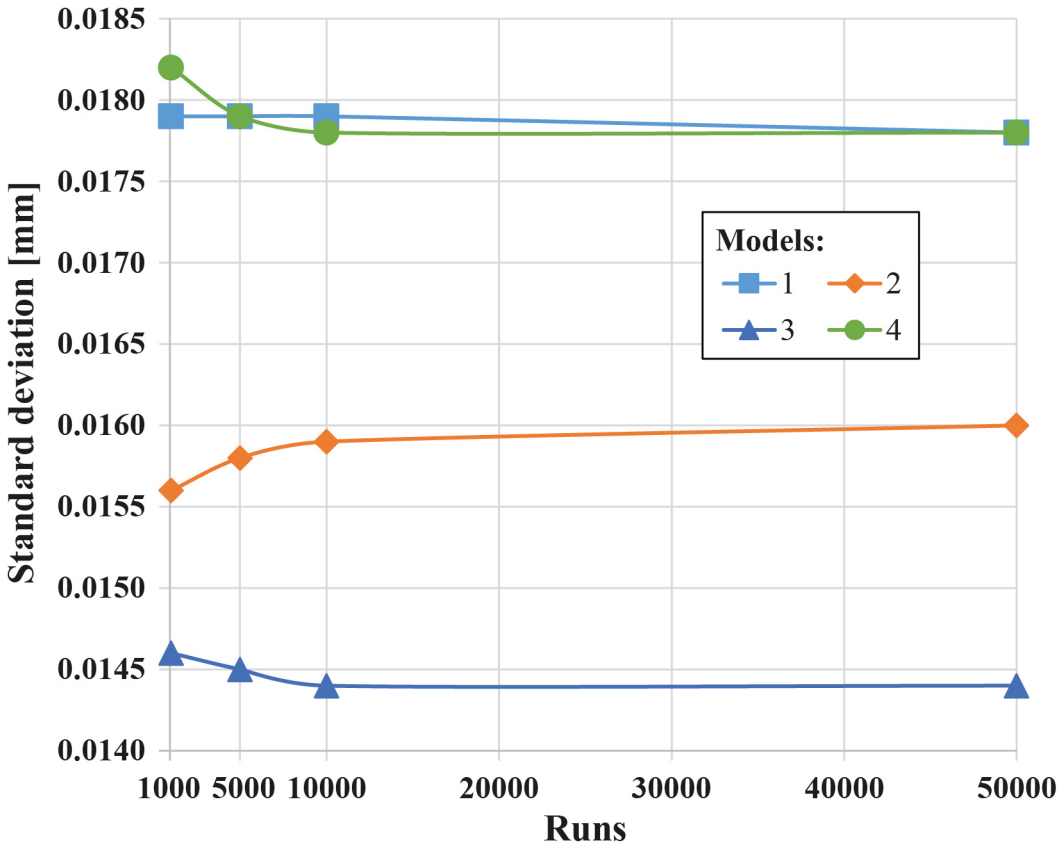

Figure 11. Results of the standard deviations due to the sensitivity analysis by considering a scale factor F=1 in all models.

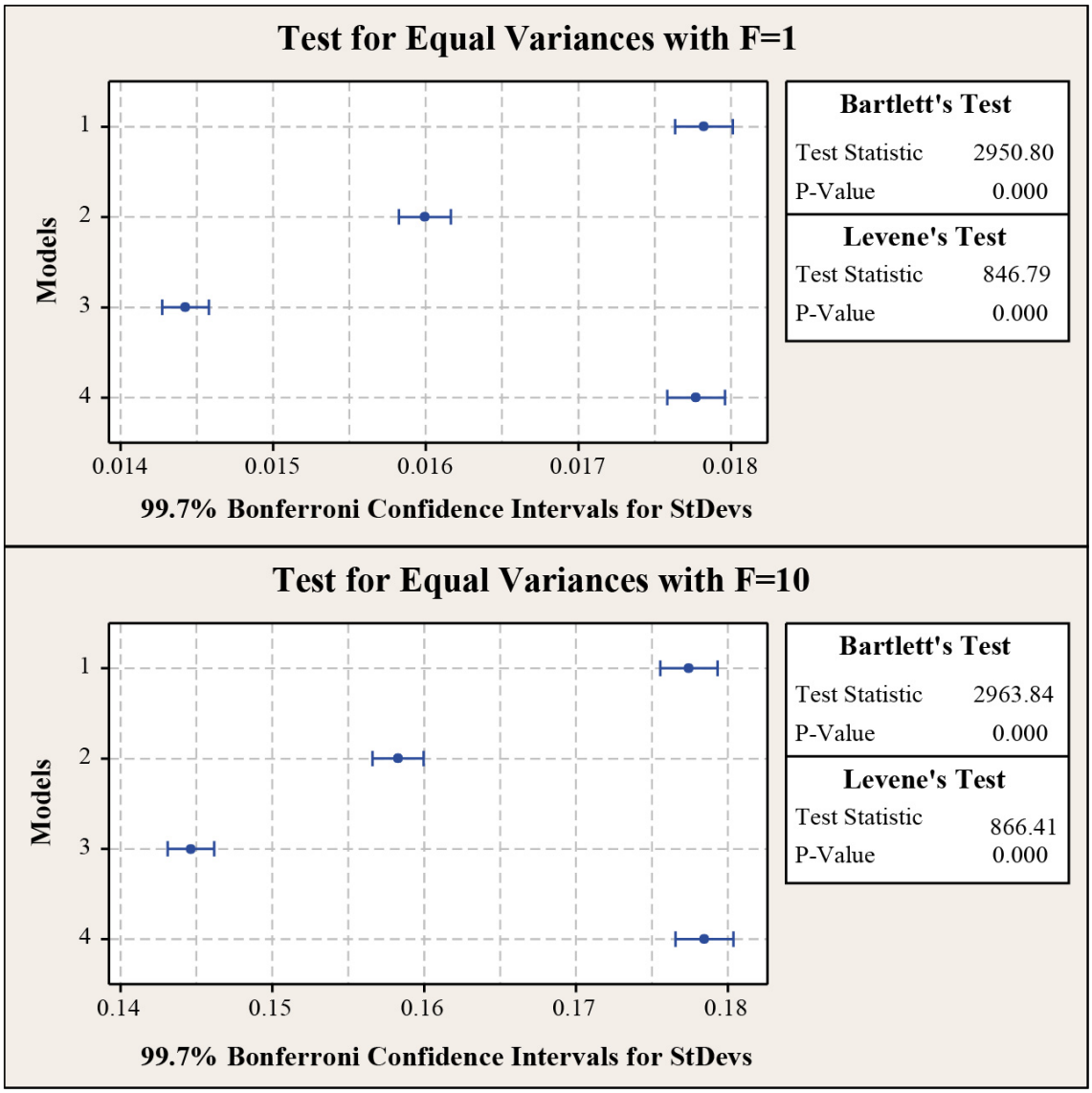

Figure 12. Tests for equal variances.

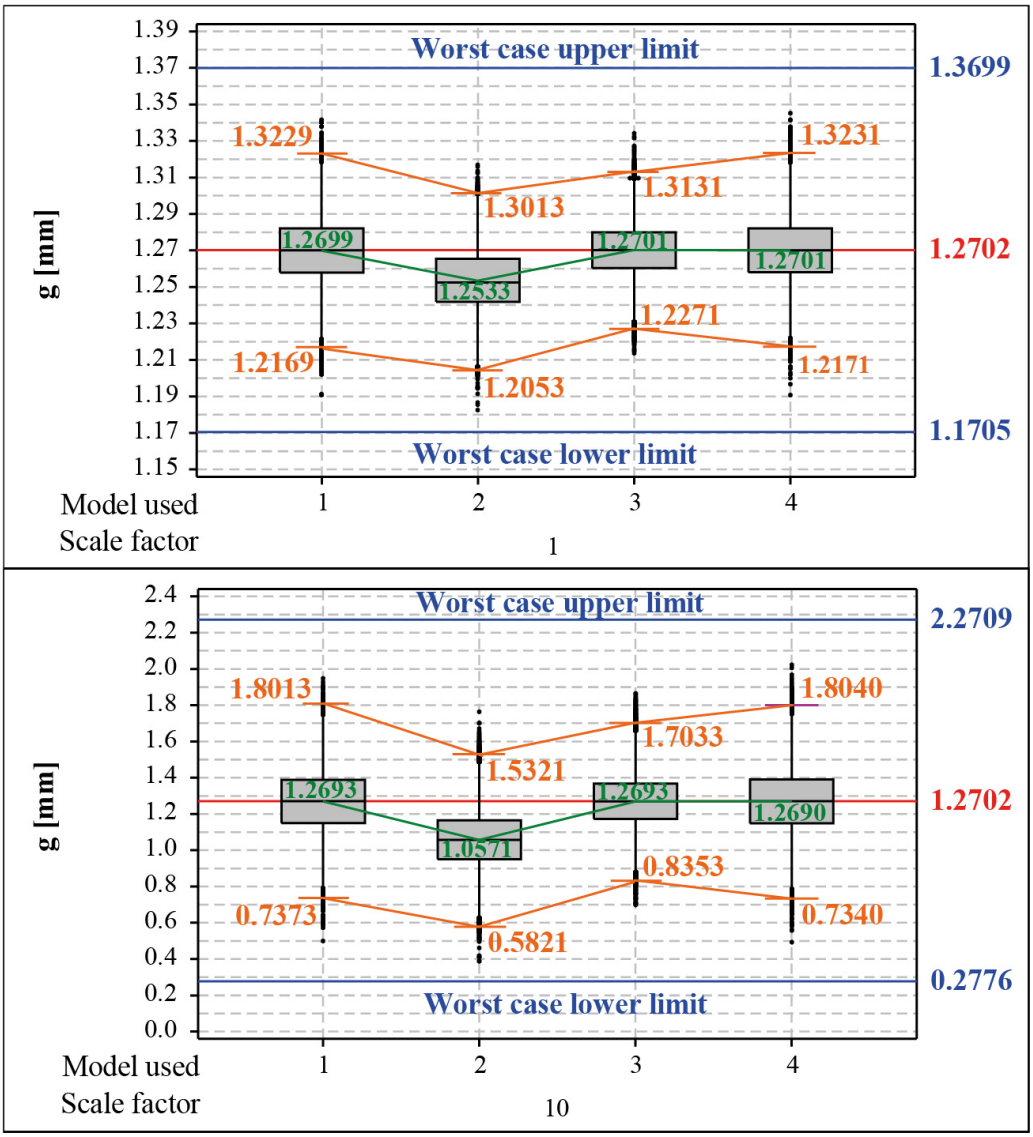

Figure 13. Boxplots of the obtained results (average value ± 3 estimated standard deviation).

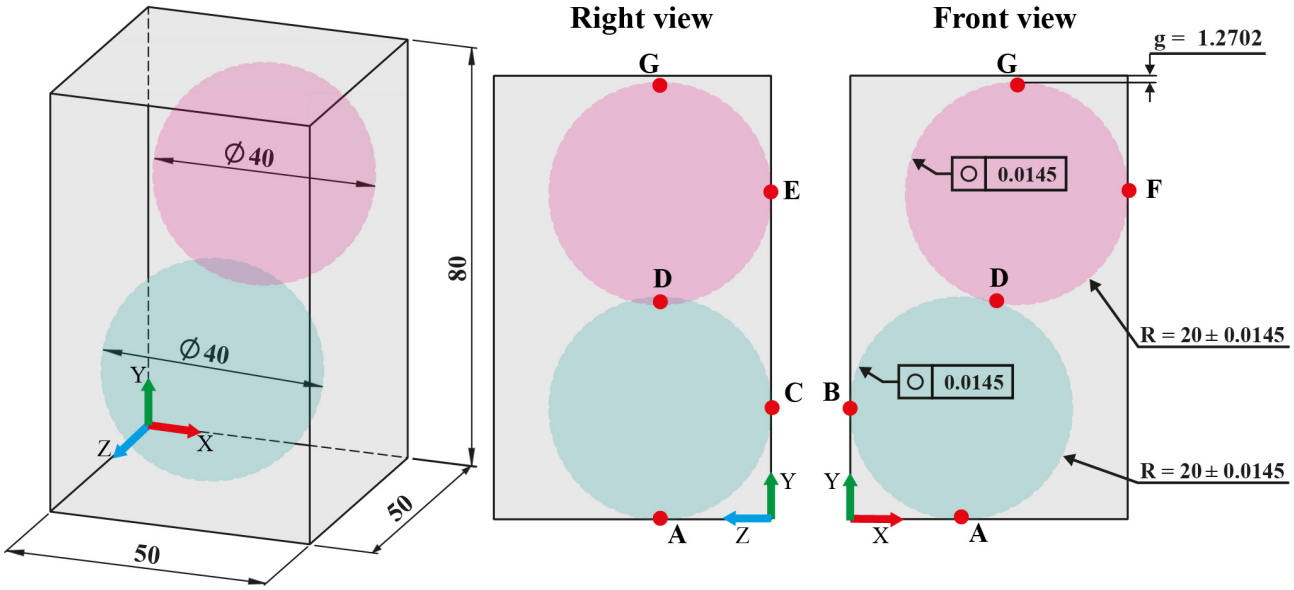

Figure 14. 3D case study (all dimensions and tolerances are in mm).

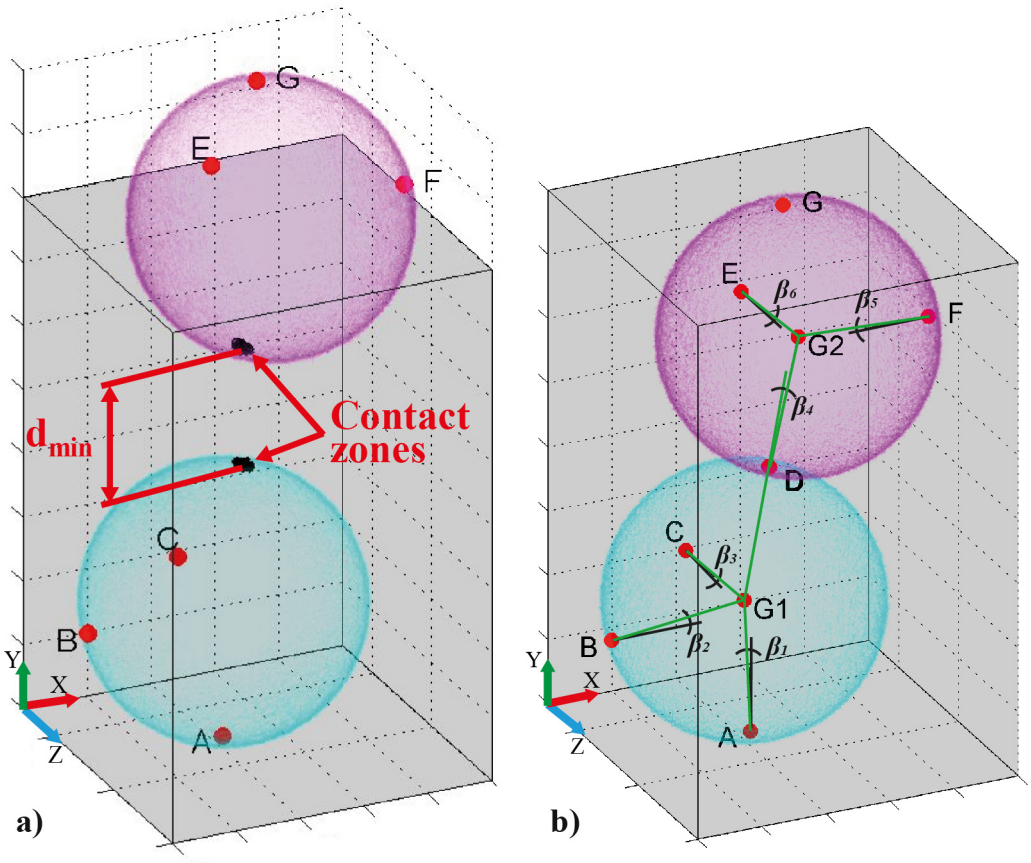

Figure 15. Approach to bring the two spheres into contact: a) contact zone and minimum distance between two circular profiles; b) tilt angles of the two spheres.

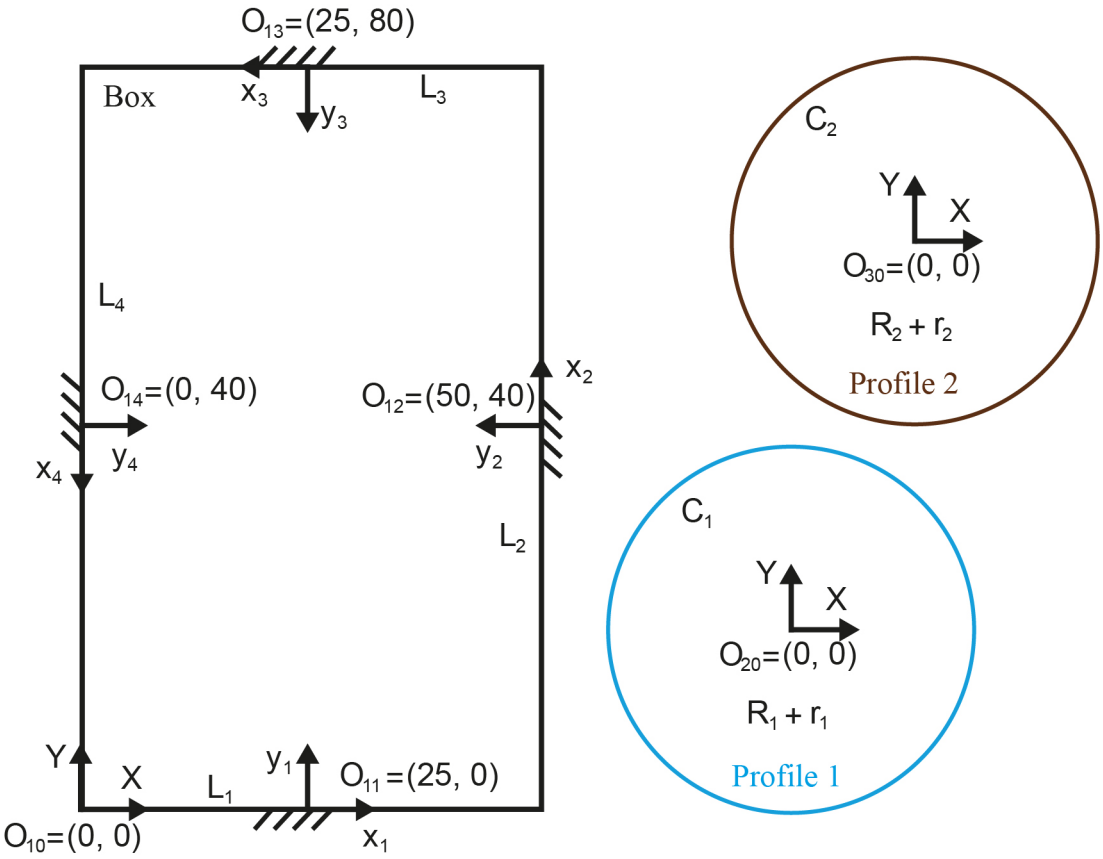

Figure 16. Local and global DRFs and features.

Table captions

Table 1. ARMAX model parameters.

Table 2. Simulation results of variational model (50000 runs).

Table 3. Simulation results of geometrical model (50000 runs).

Table 4. Comparison among models (50000 runs).

Table 5. Comparison among models on the 3D case study (10000 runs).

Table 1. ARMAX model parameters.

	$\overline{b_3}$	$\overline{b_4}$	$\overline{b_5}$	$\overline{b_6}$	$\overline{a_1}$	$\overline{a_2}$
(a)	−0.0341	0.0313	0.0080	−0.0322	0.3714	0.2723
(b)	0.0004	−0.0002	0.0001	0	0.0001	0.0003
	−0.0002	0.0004	0.0001	0	0.0001	−0.0002
	0.0001	0.0001	0.0002	0	0.0001	0
	0	0	0	0.0003	0.0003	0.0003
	0.0001	0.0001	0.0001	0.0003	0.0072	0.0012
	0.0003	−0.0002	0	0.0003	0.0012	0.0036

Table 2. Simulation results of variational model (50000 runs).

Model		F	Mean [mm]	Standard Deviation [mm]	A-squared	p-value	Skewness	Kurtosis
3	*Variational model WITHOUT manufacturing signature*	1	1.2701	0.0143	0.470	0.247	0.004	-0.039
		10	1.2693	0.1447	0.350	0.467	0.015	0.023
		50	1.2713	0.7250	0.420	0.320	0.009	0.015
		100	1.2707	1.4467	0.470	0.249	0.029	0.025
4	*Variational model WITH manufacturing signature*	1	1.2701	0.0177	0.430	0.307	0.011	-0.038
		10	1.2690	0.1783	0.830	0.033	-0.014	-0.026
		50	1.2400	0.8920	0.640	0.098	-0.001	-0.024
		100	1.1400	1.7663	2.000	<0.005	0.054	-0.022

Table 3. Simulation results of geometrical model (50000 runs).

Model		F	Mean [mm]	Standard Deviation [mm]	A-squared	p-value	Skewness	Kurtosis
1	*Geometrical model WITH manufacturing signature*	1	1.2699	0.0177	1.870	<0.005	-0.013	-0.057
		10	1.2693	0.1773	0.280	0.653	-0.018	-0.018
		50	1.2557	0.8887	1.220	<0.005	0.004	-0.061
		100	1.2153	1.7757	1.180	<0.005	0.004	-0.061
2	*Geometrical model WITHOUT manufacturing signature*	1	1.2533	0.0160	102.28	<0.005	0.017	-0.072
		10	1.0571	0.1583	0.380	0.401	0.015	0.010
		50	0.0830	0.7767	0.700	0.068	0.010	0.059
		100	-1.185	1.5307	0.870	0.025	0.027	0.055

Table 4. Comparison among models (50000 runs).

Model		F	Mean [mm]	Standard Deviation [mm]	Simulation time
1	*Geometrical model WITH manufacturing signature*	1	1.2699	0.0177	3 hours
		10	1.2693	0.1773	
2	*Geometrical model WITHOUT manufacturing signature*	1	1.2533	0.0160	2,5 hours
		10	1.0571	0.1583	
3	*Variational model WITHOUT manufacturing signature*	1	1.2701	0.0143	19 s
		10	1.2693	0.1447	
4	*Variational model WITH manufacturing signature*	1	1.2701	0.0177	3 hours
		10	1.2690	0.1783	

Table 5. Comparison among models on the 3D case study (10000 runs).

Model	**Mean [mm]**	**Standard Deviation [mm]**	**A-squared**	**p-value**	**Skewness**	**Kurtosis**	**Simulation time**
Geometrical model WITH manufacturing signature	1.2605	0.0166	1.940	0.005	-0.241	1.666	30 hours
Variational model WITHOUT manufacturing signature	1.2702	0.0144	0.430	0.309	0.017	-0.001	20 s
Variational model WITH manufacturing signature	1.2632	0.0163	0.620	0.108	-0.005	-0.127	30 hours